Royal Observatory of Belgium

Photoionization Physics in the ISM and CSM

Peter van Hoof
Royal Observatory of Belgium

Winter School on
Radiative Transfer in Stellar Environments
Liège, 2011-01-19

Royal Observatory of Belgium

Outline (1)

- Introduction / A typical spectrum
- Modeling a photoionized region / Physical conditions
- Hydrogen recombination / Case B approximation
- Extinction correction
- Strömgren sphere
- Collisional excitation
- Critical density
- Diagnostic line ratios
- Abundance determination
- Autoionization / dielectronic recombination
- Charge transfer
- Other ionization processes

Outline (2)

- Radiative pumping
- Grains / Stochastic heating
- Determining the physical conditions
- Basic PDR physics
- Some examples of applications of Cloudy
- Cloudy_3D
- The future

Royal Observatory of Belgium

Credits

Unless otherwise noted, all images and tables in this presentation are taken from:

Astrophysics of Gaseous Nebulae and Active Galactic Nuclei (2nd ed.)

Donald E. Osterbrock & Gary J. Ferland

University Science Books, ISBN 1-891389-34-3

http://www.agn3.org/

The books is commonly referred to as AGN3 and is an excellent text book for those wishing to read more about the topics discussed in this presentation.

In some section suggestions for further reading will be indicated as [AGN3: x.y].

Royal Observatory of Belgium

Introduction (1)

Royal Observatory of Belgium

Photoionization is a common process in the interstellar medium (ISM) and in circumstellar material (CSM). It happens when gas is being irradiated and ionized by photons from an external source.

The ionizing source is usually a star or an ensamble of stars, but could also be an accretion disk.

Typically the distance of the ionizing source is much larger than the diameter of the source, implying that its radiation field is strongly spherically diluted when it reaches the gas.

Some classical examples of photoionized sources are:

- Regions of massive star formation
- Planetary Nebulae
- Novae / Supernovae
- Active Galactic Nuclei

Introduction (2)

This is the star forming region N90 in the Small Magellanic Cloud. The cluster of blue massive stars that is ionizing the cloud (with T_{eff} = 30–50 kK) is clearly visible in the center. The radiation pressure and the winds from these stars have blown a nearly spherical bubble in the molecular cloud from which they formed. [AGN3: 1.5]

Image Credit: NASA, ESA and the Hubble Heritage Team (STScI/AURA)-ESA/Hubble Collaboration.

Royal Observatory of Belgium

Introduction (3)

Royal Observatory of Belgium

This is the PN NGC 6302. It is very young and dense. The central star is one of the hottest known (> 200 kK) and is on its way to become a white dwarf. The current mass of the star is 0.64 Msol, but the original mass must have been much higher. Most of the stellar material has been expelled and now forms the PN. It has a bipolar (hourglass) shape with a marked equatorial density enhancement. [AGN3: 1.6]

Image Credit: NASA, ESA and the Hubble SM4 ERO Team.

Introduction (4)

Royal Observatory of Belgium

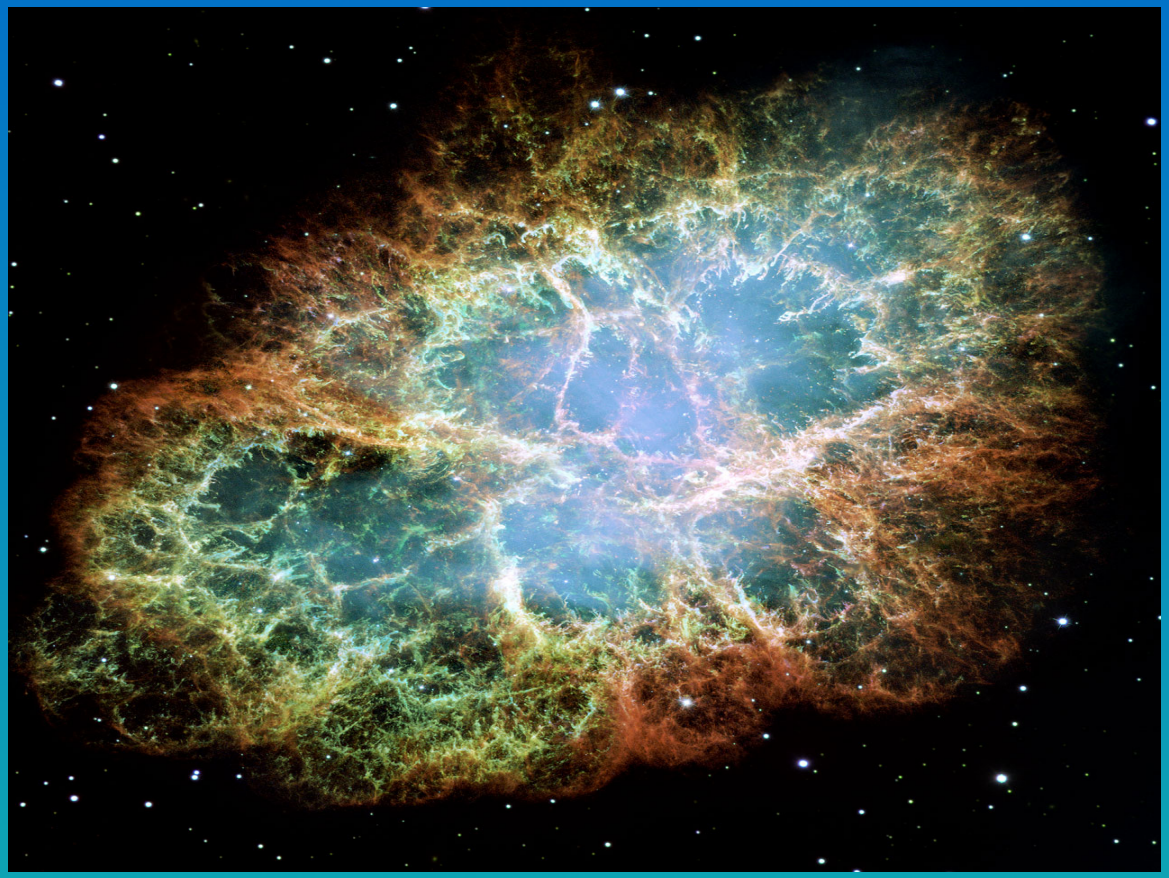

This is the Crab Nebula (SN 1054), a supernova remnant. It is a strong X-ray and gamma-ray source. The central star is a pulsar: a neutron star with a strong magnetic field. It is obvious that the nebular material that was ejected in the supernova explosion is extremely filamentary. [AGN3: 1.7]

Image Credit: NASA, ESA and Allison Loll/Jeff Hester (Arizona State University).

Introduction (5)

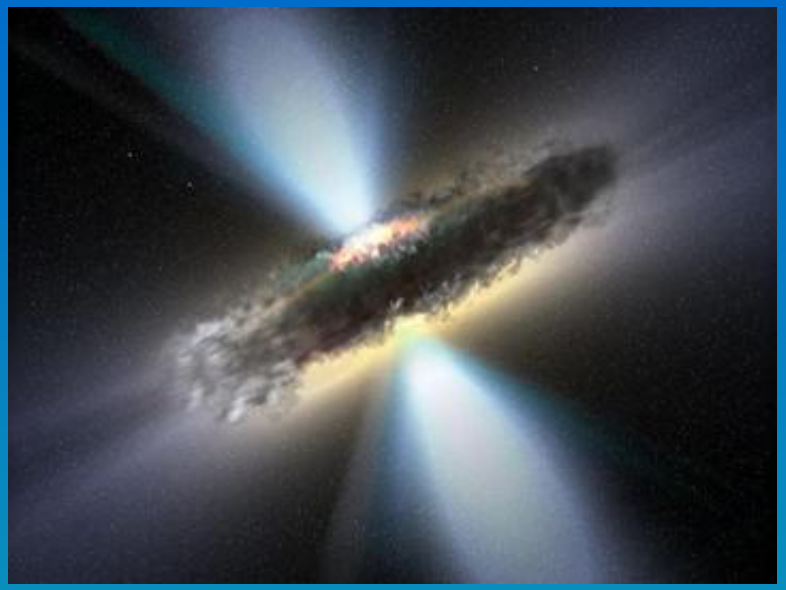

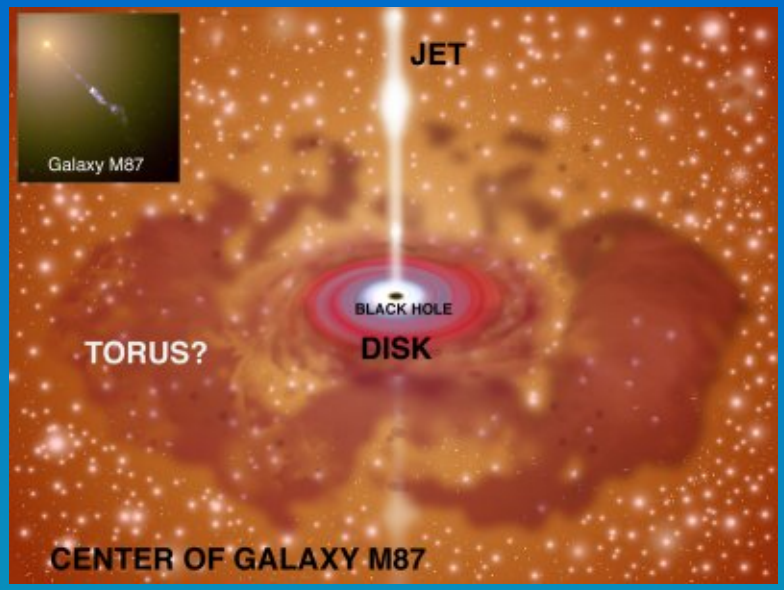

These are artists impressions of the central engine of an Active Galactic Nucleus (AGN). At the center is a supermassive black hole surrounded by an accretion disk that is heated to X-ray temperatures. These objects are also strong synchroton sources, the origin of which is not clear. Surrounding this is a fat torus of (possibly molecular) gas that is also very dusty which may obscure the central engine from certain viewing angles. The central engine often drives powerful jets that can form giant radio lobes. [AGN3: 1.8]

Image Credit: The Gemini Observatory.

Introduction (6)

Royal Observatory of Belgium

This list of photoionized objects is certainly not exhaustive. Other types may e.g. include Wolf-Rayet nebulae.

From what we have seen so far, we can draw the following conclusions:

- We have a wide variety of ionizing sources showing great differences in the level of excitation. The objects shown were roughly in order of increasing excitation.
- The ionized gas can have very different morphologies, ranging from roughly spherical or elliptical bubbles, to bipolar shapes, tori, or even completely irregular shapes. The gas can be smooth, filamentary or clumpy.
- The gas may originate from the ionizing star, in which case it often has unusual abundance patterns (in extreme cases H- or even He-deficient), but it may also be the gas from which the ionizing source formed. In some cases the gas and ionizing source are not related at all.
- The gas may contain dust grains.

Introduction (7)

When the ionized region is optically thick to ionizing radiation (in this case we speak of an ionization bounded nebula) there will be gas outside the ionized region where molecular chemistry can take place. This region is called a PDR, which stands either for Photo-Dissociation Region or Photon-Dominated Region. It has the following schematic structure: [AGN3: 8]

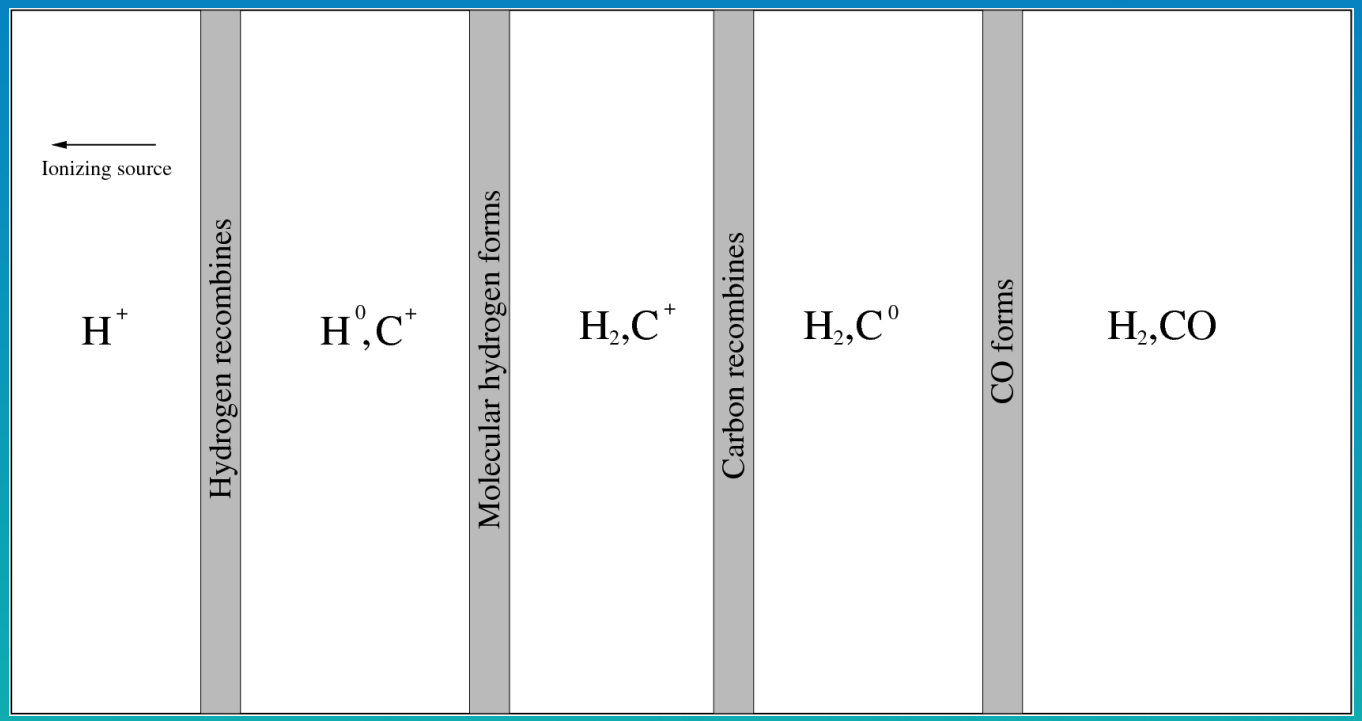

Image credit: P. van Hoof

A typical spectrum (1)

Shown here is a typical optical spectrum of a photoionized region, in this case the Orion nebula. What we see are strong emission lines: permitted lines from hydrogen (and also helium, but those lines are too weak to see on this scale) and a variety of forbidden lines. The continuum is difficult to detect. In the UV we see the SED from the ionizing stars.

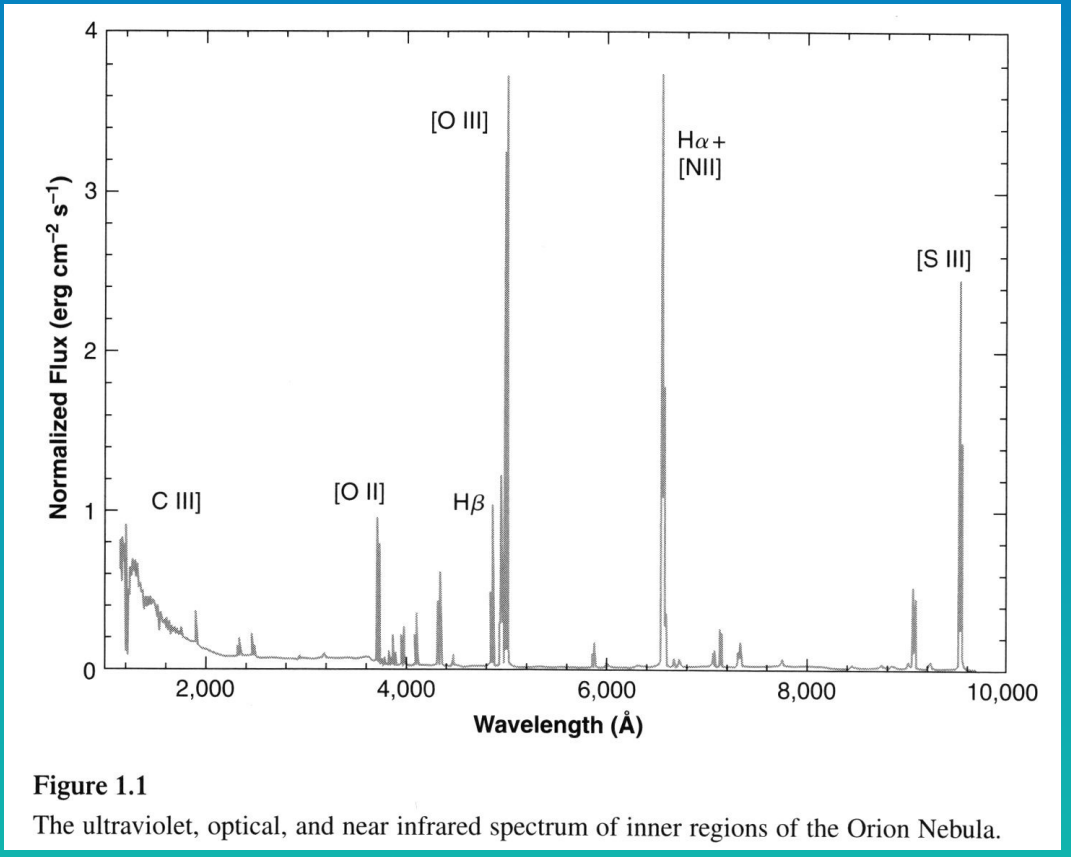

Figure 1.1
The ultraviolet, optical, and near infrared spectrum of inner regions of the Orion Nebula.

A typical spectrum (2)

Shown here is a model spectrum of a photoionized H II region on a logarithmic scale. This model has been calculated with the photionization code Cloudy. Prominently visible are the strong far-IR emission from the grains and the far-IR fine structure lines. In the far-IR and (sub-) mm regime one would also expect a variety of molecular lines (e.g. CO). The upcoming release of Cloudy can model those as well, but they are missing in this plot.

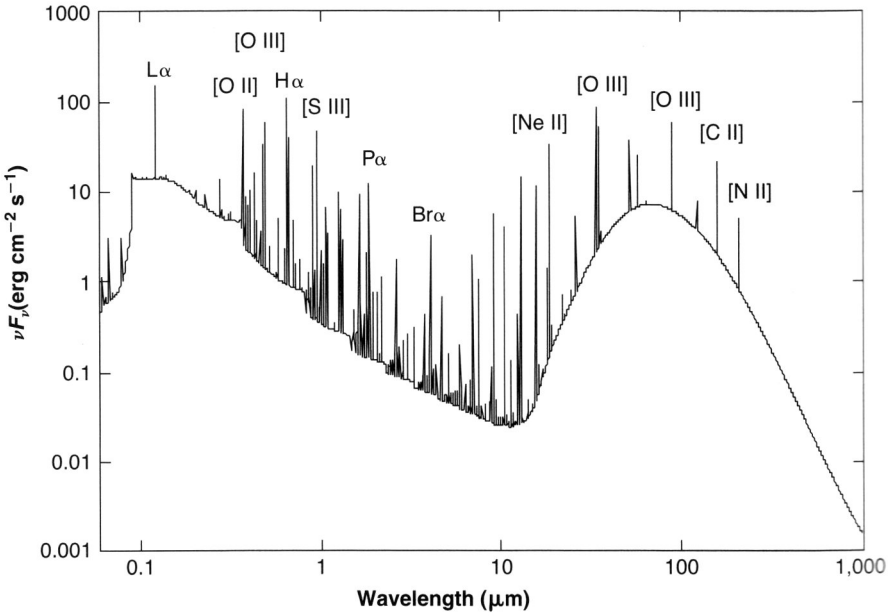

Figure 8.1

The lines and continuum transmitted through the hydrogen ionization front of the simple model H II region show in Figure 2.3 and Figure 7.9. Thermal emission by embedded grains produces the peak near λ100 μm, while starlight and atomic processes in the H II region produce the peak near λ0.1 μm. All of the labeled lines have been measured in the Orion Nebula.

Royal Observatory of Belgium

Modeling a photoionized region

Royal Observatory of Belgium

What we have seen in the introduction already gives us some idea of the challenges involved in understanding photoionized regions: there is a wide variety of ionizing sources, and also the morphology of the gas can be very different from one source to another. Furthermore, the gas composition may be very different from a standard solar composition. Hydrodynamic interactions, including shocks, may complicate things further.

A sophisticated code is needed to handle all these challenges. Several codes are available, each with their own strengths and weaknesses. The most widely used code is Cloudy. This is an open source C++ code which can be freely downloaded from:

http://nublado.org

The great strength of this code is its detailed, state-of-the-art treatment of the various microphysical processes and the fact that it can produce a unified model of the ionized region and the PDR / molecular region. Most likely its biggest weakness is that it is a 1D spherically symmetric code. It also doesn't treat shocks.

Physical conditions (1)

Royal Observatory of Belgium

The photoionized gas can be characterized by an electron temperature and the abundances of each ionization stage of every element (the ionization structure). The ionization structure implies an electron density (charge conservation). Each ion is characterized by the level populations of each of its electronic states.

It is commonly assumed that the electrons have a perfect Maxwellian distribution. Deviations do exist near strong temperature gradients (solar corona) and from secondary electrons due to cosmic ray ionizations (molecular regions).

The dominant processes determining the ionization structure are photoionization and its inverse process, radiative recombination. Other processes play a role too, they will be discussed later.

It is commonly assumed that the ionization structure is in equilibrium with the radiation field (steady state). This is often a good approximation, but deviations are known (e.g., the guitar nebula, recombining PNe).

Physical conditions (2)

Royal Observatory of Belgium

The dominant processes determining the level populations of the ions are collisional (de-) excitation, spontaneous and induced radiative decay, continuum or line pumping and radiative cascades following recombination.

As was mentioned before, the radiation field is usually strongly diluted ($T_{rad} >> T_{ed}$) and the gas density is usually low (typically $10^0 - 10^8$ cm^{-3}) so that neither the radiation field nor the collisions in the gas can establish LTE. Hence calculations of a photoionized plasma need to be done in full non-LTE.

Excitation and de-excitation processes generally are very fast, so the level populations are determined by balancing the rate equations for each of these processes (steady-state).

The electron temperature is determined by balancing heating and cooling processes. Each of these processes is a function of temperature, so we search for a temperature such that the sum of all the heating processes and all the cooling processes match exactly. Usually there is only one solution, but there can be multiple solutions, in which case the gas is bistable.

Hydrogen recombination (1)

Let us consider the simplified example of a homogeneous pure hydrogen cloud ionized by a central source.

We can define the number of hydrogen ionizing photons Q(H) (units photon s^{-1}) emitted by the central source as:

$$Q(\mathrm{H}^0) = \int_{\nu_0}^{\infty} \frac{L_\nu}{h\nu} d\nu$$

Here ν_0 is the threshold frequency for the ionization process, corresponding to the ionization potential of hydrogen (13.6 eV).

Each time a hydrogen atom is ionized, a proton and an electron will form. These will eventually recombine radiatively. Sometimes the recombining electron will go straight into the ground state, but most of the time the recombined hydrogen atom will be in an excited state.

The excited state will decay radiatively, usually via intermediate states, until it reaches either the 1s or 2s state. [AGN3: 2.1, 2.2]

Hydrogen recombination (2)

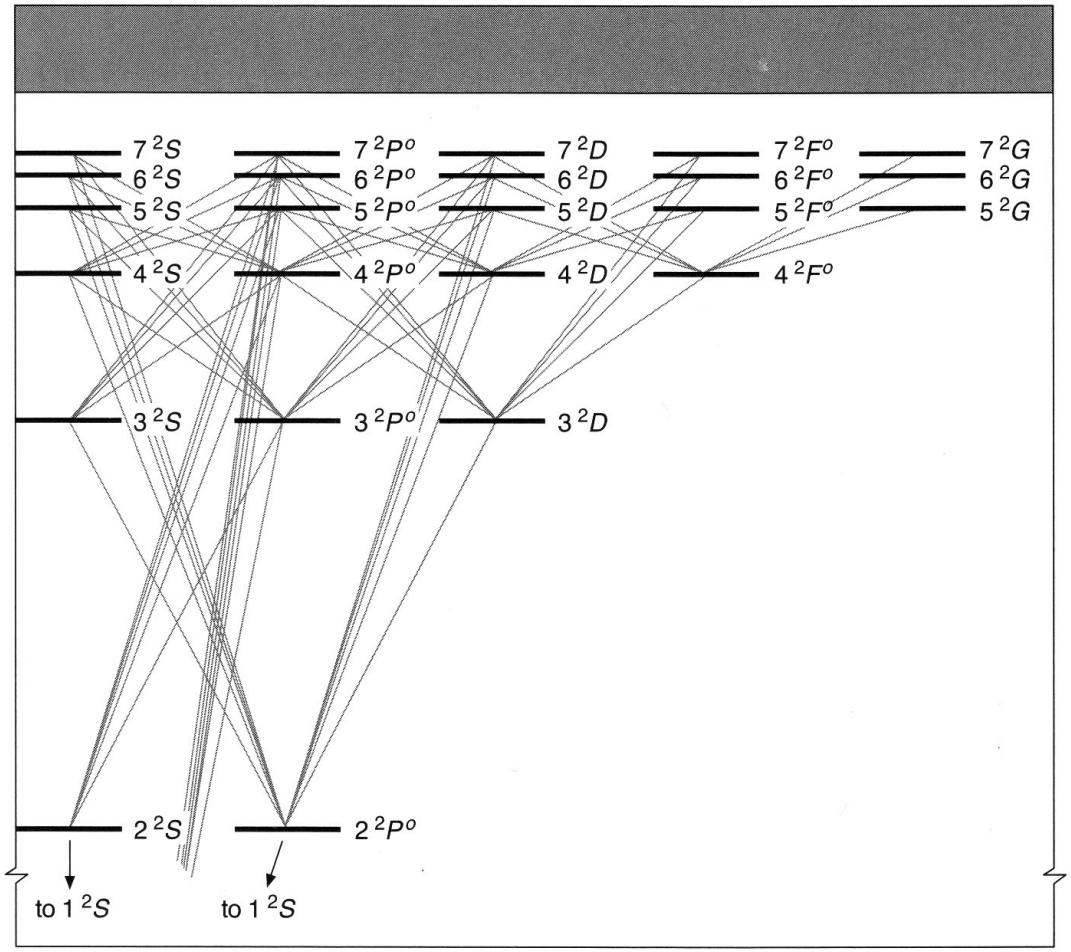

Figure 2.1

Partial energy-level diagram of H I, limited to $n \leq 7$ and $L \leq G$. Permitted radiative transitions to levels $n < 4$ are indicated by solid lines.

Hydrogen recombination (3)

Recombinations directly to the ground state will only produce another ionizing photon. It is the exact inverse of the ionizing process. The number of ionizing photons will remain the same.

Recombinations into higher levels will destroy the ionizing photon: it will be split up in photons of lower energy, none of which are capable of ionizing hydrogen again. For example, recombination into the n=3 state will emit a non-ionizing photon which can be followed by a 3-1 transition (Lyβ) or a 3-2 (Hα) transition followed by 2-1 (Lyα).

The Lyβ photon can be absorbed again by hydrogen, again resulting either in the emission of Lyβ or Hα+Lyα, but sooner or later the latter will happen. To first order, the Lyα photon cannot be destroyed, it can only be absorbed and re-emitted as a Lyα photon (this neglects background opacities such as from grains).

This results in the important rule that every photoionization of hydrogen is eventually followed by the emission of exactly one Lyα photon. Since the Lyα line can be observed, this allows us to measure Q(H) directly assuming that the cloud is optically thick.

Royal Observatory of Belgium

Hydrogen recombination (4)

Royal Observatory of Belgium

Table 2.1

Recombination coefficients (in $cm^3\ s^{-1}$) $\alpha_n\ ^2L$ for H

	5,000 K	10,000 K	20,000 K
$\alpha_{1\ ^2S}$	2.28×10^{-13}	1.58×10^{-13}	1.08×10^{-13}
$\alpha_{2\ ^2S}$	3.37×10^{-14}	2.34×14^{-14}	1.60×10^{-14}
$\alpha_{2\ ^2P^o}$	8.33×10^{-14}	5.35×10^{-14}	3.24×10^{-14}
$\alpha_{3\ ^2S}$	1.13×10^{-14}	7.81×10^{-15}	5.29×10^{-15}
$\alpha_{3\ ^2P^o}$	3.17×10^{-14}	2.04×10^{-14}	1.23×10^{-14}
$\alpha_{3\ ^2D}$	3.43×10^{-14}	1.73×10^{-14}	9.49×10^{-15}
$\alpha_{4\ ^2S}$	5.23×10^{-15}	3.59×10^{-15}	2.40×10^{-15}
$\alpha_{4\ ^2P^o}$	1.51×10^{-14}	9.66×10^{-15}	5.81×14^{-15}
$\alpha_{4\ ^2D}$	1.90×10^{-14}	1.08×10^{-14}	5.68×10^{-15}
$\alpha_{4\ ^2F^o}$	1.09×10^{-14}	5.54×10^{-15}	2.56×10^{-15}
$\alpha_{10\ ^2S}$	4.33×10^{-16}	2.84×10^{-16}	1.80×10^{-16}
$\alpha_{10\ ^2G}$	2.02×10^{-15}	9.28×10^{-16}	3.91×10^{-16}
$\alpha_{10\ ^2M}$	2.7×10^{-17}	1.0×10^{-17}	4.0×10^{-18}
α_A	6.82×10^{-13}	4.18×10^{-13}	2.51×10^{-13}
α_B	4.54×10^{-13}	2.59×10^{-13}	1.43×10^{-13}

The recombination coefficients into the various hydrogen levels have a fairly similar dependence on T_e, resulting in the fact that the distribution of photons emitted during the recombination cascade (the recombination spectrum) is only very weakly dependent on T_e.

Hydrogen recombination (5)

Royal Observatory of Belgium

The cascade down is fast (the lifetime of the lower excited levels is typically less than 1 μs, but for high levels this is much longer). Nevertheless it can happen that an electron collides before the radiative decay occurs, causing a transition.

This is important in two cases: transitions between states with the same principal quantum number n and between adjacent states with high n. Because of the small energy difference, the collision rates are fast, in both cases causing relative level populations that are close to LTE.

Since the electron collisions either have very little effect (between adjacent low-lying states) or cause relative level populations that are close to LTE, the recombination spectrum of hydrogen only has a weak dependence on the electron density.

If you make the assumption that the Lyman lines are optically thick and all other hydrogen lines are optically thin, you can calculate the relative intensities of the various hydrogen lines. This is called the Case B approximation. [AGN3: 4.2]

Case B approximation

Table 4.4
H I recombination lines (Case B)

	T								
	5,000 K			10,000 K			20,000 K		
n_e (cm^{-3})	10^2	10^4	10^6	10^2	10^4	10^6	10^2	10^4	10^6
$4\pi j_{H\beta}/n_e n_p$ (10^{-25} erg cm^3 s^{-1})	2.20	2.22	2.29	1.23	1.24	1.25	0.658	0.659	0.661
$\alpha^{eff}_{H\beta}$ (10^{-14} cm^3 s^{-1})	5.37	5.43	5.59	3.02	3.03	3.07	1.61	1.61	1.62
Balmer-line intensities relative to Hβ									
$j_{H\alpha}/j_{H\beta}$	3.041	3.001	2.918	2.863	2.847	2.806	2.747	2.739	2.725
$j_{H\gamma}/j_{H\beta}$	0.458	0.460	0.465	0.468	0.469	0.471	0.475	0.476	0.476
$j_{H\delta}/j_{H\beta}$	0.251	0.253	0.258	0.259	0.260	0.262	0.264	0.264	0.266
$j_{H10}/j_{H\beta}$	0.0515	0.0520	0.0616	0.0530	0.0533	0.0591	0.0540	0.0541	0.0575
$j_{H15}/j_{H\beta}$	0.01534	0.01628	0.02602	0.01561	0.01620	0.02147	0.01576	0.01612	0.01834
$j_{H20}/j_{H\beta}$	0.00657	0.00819	0.01394	0.00662	0.00755	0.01058	0.00664	0.00717	0.00832

Case B is an excellent approximation for most photoionized environments such as star forming regions and PNe. However, modern photoionization codes such as Cloudy can do a detailed calculation on the fly, including more microphysics and without the need for assumptions on the line optical depth of the various hydrogen lines.

Extinction correction

Royal Observatory of Belgium

An observed spectrum will suffer from dust extinction. A large fraction of this will be interstellar extinction, but some of this can also be internal extinction in the nebula itself.

Before you can analyze the spectrum, you first need to correct for the extinction. A commonly used method is the Balmer decrement method. Here we use the fact that the Hα/Hβ line flux ratio has an intrinsic value ~ 2.85 almost independent of electron temperature and density. By comparing the observed ratio with the theoretical value, you can determine the extinction parameter c(Hβ) using:

$$\log [\ F(H\alpha)/F(H\beta)\ ] = \log(2.85) + 0.334\ c(H\beta)$$

Note that this method implicitly assumes that the Balmer lines are optically thin. The constant 0.334 depends to some extent on the interstellar extinction law.

Other methods are also in use, e.g. by comparing the observed Hβ flux with the optically thin free-free radio flux of the nebula.

Strömgren sphere (1)

Royal Observatory of Belgium

Using the information we have gathered so far, we can now calculate the size of the region that is being ionized by the central source. Let us recap the assumptions:

- We have homogeneous and isothermal pure hydrogen gas that is assumed to be fully ionized everywhere inside the ionized region. For lower excitation sources this is an excellent approximation.
- The central source produces ionizing photons at a rate Q(H), all of which are absorbed.
- The ionized region is in a time-steady state, i.e. every ionization is balanced by a recombination.

Using this we can easily see that the size of the ionized region is given by: [AGN3: 2.3]

$$Q(\mathrm{H}^0) = \frac{4\pi}{3} r_1^3 n_{\mathrm{H}}^2 \alpha_B$$

Strömgren sphere (2)

This ionized region is often referred to as a Strömgren sphere, and the radius of the region (r_1 in the previous equation) as the Strömgren radius. The table below shows the values of the Strömgren radius for a range of hot stars assuming a typical ISM density of 1 cm^{-3} and T_e = 7500 K.

Table 2.3

Calculated Strömgren radii as function of spectral types spheres

Spectral type	T_* (K)	M_V	log $Q(H^0)$ (photons/s)	log $n_e n_p r_1^3$ n in cm^{-3}; r_1 in pc	log $n_e n_p r_1^3$ n in cm^{-3}; r_1 in pc	r_1 (pc) $n_e = n_p$ = 1 cm^{-3}
O3 V	51,200	−5.78	49.87	49.18	6.26	122
O4 V	48,700	−5.55	49.70	48.99	6.09	107
O4.5 V	47,400	−5.44	49.61	48.90	6.00	100
O5 V	46,100	−5.33	49.53	48.81	5.92	94
O5.5 V	44,800	−5.22	49.43	48.72	5.82	87
O6 V	43,600	−5.11	49.34	48.61	5.73	81
O6.5 V	42,300	−4.99	49.23	48.49	5.62	75
O7 V	41,000	−4.88	49.12	48.34	5.51	69
O7.5 V	39,700	−4.77	49.00	48.16	5.39	63
O8 V	38,400	−4.66	48.87	47.92	5.26	57
O8.5 V	37,200	−4.55	48.72	47.63	5.11	51
O9 V	35,900	−4.43	48.56	47.25	4.95	45
O9.5 V	34,600	−4.32	48.38	46.77	4.77	39
B0 V	33,300	−4.21	48.16	46.23	4.55	33
B0.5 V	32,000	−4.10	47.90	45.69	4.29	27
O3 III	50,960	−6.09	49.99	49.30	6.38	134
B0.5 III	30,200	−5.31	48.27	45.86	4.66	36
O3 Ia	50,700	−6.4	50.11	49.41	6.50	147
O9.5 Ia	31,200	−6.5	49.17	47.17	5.56	71

Note: $T = 7{,}500$ K assumed for calculating α_B.

Collisional excitation (1)

Royal Observatory of Belgium

Both H and He have no low-lying excited states that can easily be collisionally excited. The lowest excited level in H has an energy of 10.2 eV, in He^0 it is 19.8 eV, and in He^+ it is 40.8 eV.

Most photoionized sources have very similar electron temperatures (more on that later), typically between 8 and 20 kK with a canonical value of 10 kK. This corresponds to:

$$kT_e = 0.86 \text{ eV}, \lambda = hc/kT_e = 1.44 \text{ μm}$$

Hence only electrons in the extreme high energy tail of the Maxwell distribution can excite H or He.

For ions with open p or d shells the situation is very different. These have low-lying metastable states can that can readily be excited. We will look at the O^{++} ion that has a $2s^2.2p^2$ ground configuration. It has 5 metastable states as shown in the following figure. Metastable states have no “allowed” E1 transitions to lower states, but do have “forbidden” M1 and/or E2 transitions. The “forbidden” transitions are not really forbidden, but have much lower Einstein-A's than “allowed” transitions.

Collisional excitation (2)

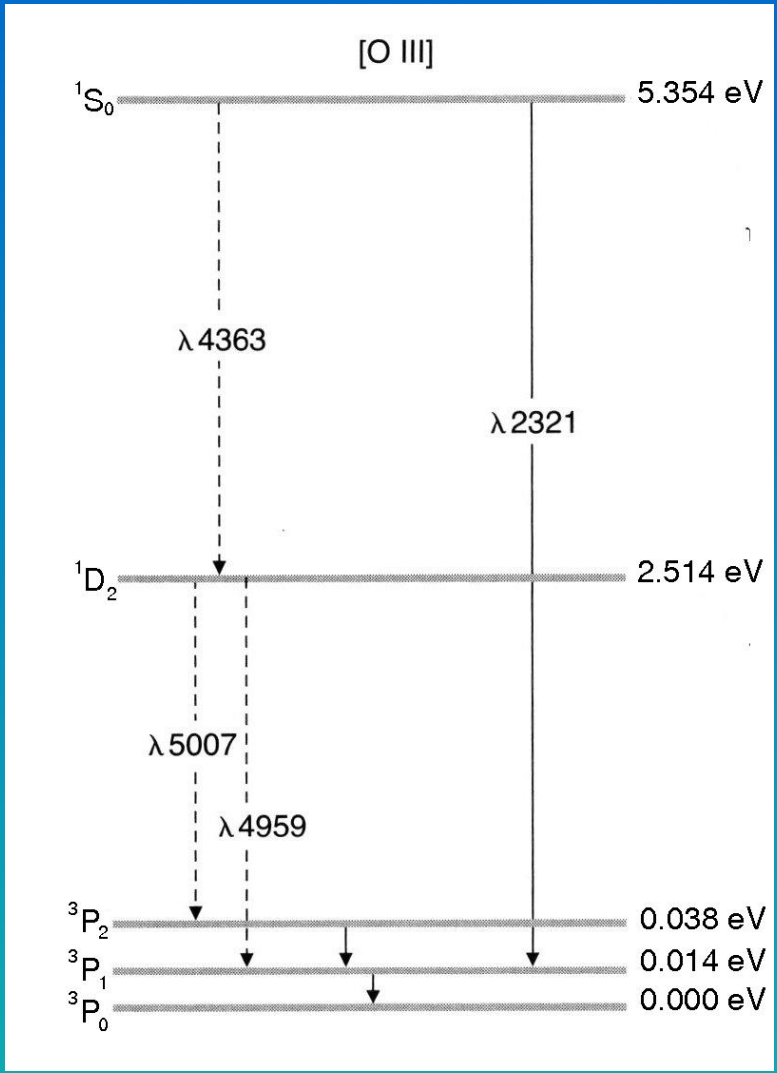

The $^1D_2$ state can easily be excited in typical photoionized gas, resulting in very strong [O III] 4959 and 5007 Å lines. The photons that were created in this process remove kinetic energy from the electron pool and are said to cool the gas. The important cooling lines in photoionized gas (like these two [O III] lines) typically are forbidden lines. [AGN3: 3.5]

The recombination lines of H and He do *not* cool the gas as they were not collisionally excited. They get their energy from the radiation field of the ionizing source through photoionization. The bound-free continuum does cool the gas. [AGN3: 3.3]

Collisional excitation (3)

Royal Observatory of Belgium

The important cooling lines come from levels with energies a few times kTe. They can be readily excited, but the excitation rate still has an exponential dependence ~ $\exp(-\Delta E/kT_e)$.

Using this information we can understand why many photoionized sources have very similar electron temperatures. Let us assume we have a plasma in equilibrium and we try to raise the temperature by dumping more energy in the plasma. The kinetic energy of the electrons will go up and the excitation rate of the cooling lines will rise exponentially. Hence the cooling lines will also become stronger.

The net result of our injection of energy is that the cooling lines become stronger which radiate most of that energy away again. Only a small fraction will remain as additional kinetic energy of the gas. Hence the temperature will only have been raised a little bit.

This is called the thermostat effect and explains why most photoionized sources have very similar temperatures: the heating rates may differ quite a bit, but the exponential dependence of the cooling rate on T_e forces the temperatures to be similar.

Critical density

The critical density of a level is defined as the electron density where the collisional rate to any other level matches the total radiative rate to all lower levels. Below the critical density radiative decay will dominate, above collisional de-excitation (collisional quenching of the line). [AGN3: 3.5]

$$n_c(i) = \sum_{j<i} A_{ij} \Big/ \sum_{j \neq i} q_{ij}$$

Table 3.15

Critical densities for collisional deexcitation

Ion	Level	n_e (cm^{-3})	Ion	Level	n_e (cm^{-3})
C II	$^2P^o_{3/2}$	5.0×10^1	O III	$^1D_2$	6.8×10^5
C III	$^3P^o_2$	5.1×10^5	O III	$^3P_2$	3.6×10^3
N II	$^1D_2$	6.6×10^4	O III	$^3P_1$	5.1×10^2
N II	$^3P_2$	3.1×10^2	Ne II	$^2P^o_{1/2}$	7.1×10^5
N II	$^3P_1$	8.0×10^1	Ne III	$^1D_2$	9.5×10^6
N III	$^2P^o_{3/2}$	1.5×10^3	Ne III	$^3P_0$	3.1×10^4
N IV	$^3P^o_2$	1.1×10^6	Ne III	$^3P_1$	2.1×10^5
O II	$^2D^o_{3/2}$	1.5×10^4	Ne V	$^1D_2$	1.3×10^7
O II	$^2D^o_{5/2}$	3.4×10^3	Ne V	$^3P_2$	3.5×10^4
			Ne V	$^3P_1$	6.2×10^3

NOTE: All values are calculated for $T = 10{,}000$ K.

Diagnostic line ratios (1)

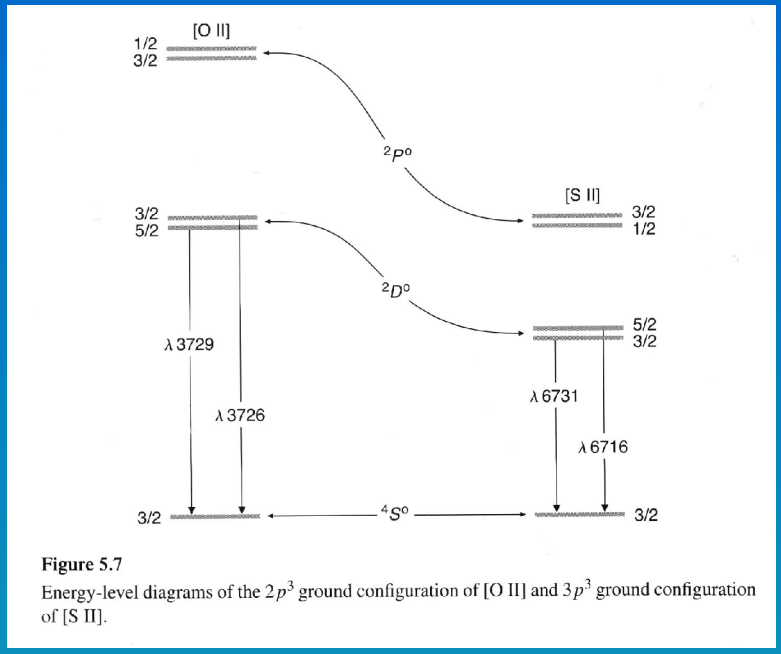

Figure 5.7
Energy-level diagrams of the $2p^3$ ground configuration of [O II] and $3p^3$ ground configuration of [S II].

Density sensitive line ratios arise when you have a doublet of lines coming from closely spaced levels which have a different critical density. Examples are the [O II] and [S II] lines shown above, but others exist. The fact that the levels are closely spaced minimizes differences in collisional excitation of the levels and hence minimizes the temperature dependence of the line ratio. [AGN3: 5.6]

Diagnostic line ratios (2)

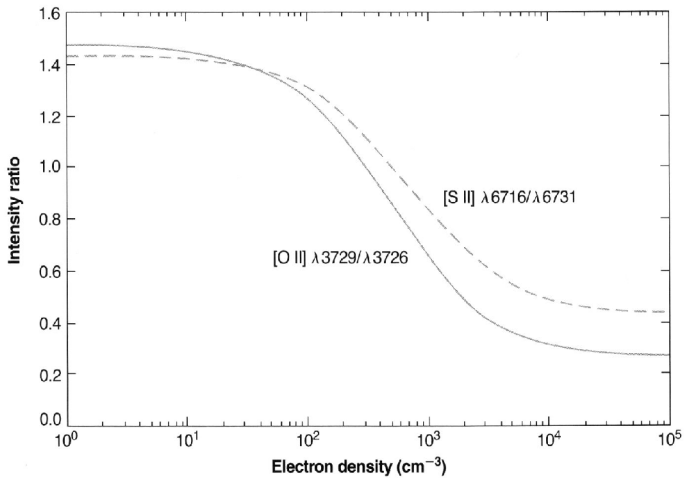

Figure 5.8

Calculated variation of [O II] (*solid line*) and [S II] (*dashed line*) intensity ratios as functions of n_e at T = 10,000 K. At other temperatures the plotted curves are very nearly correct if the horizontal scale is taken to be $n_e(10^4/T)^{1/2}$.

If the density is well below the lowest critical density, or well above the highest, the line ratio will be nearly constant. In-between the observed line ratio can be used to derive the electron density in the line forming region.

Different line ratios can be sensitive to a different range in density. Typically line ratios from higher ionization stages will be sensitive to higher densities.

Diagnostic line ratios (3)

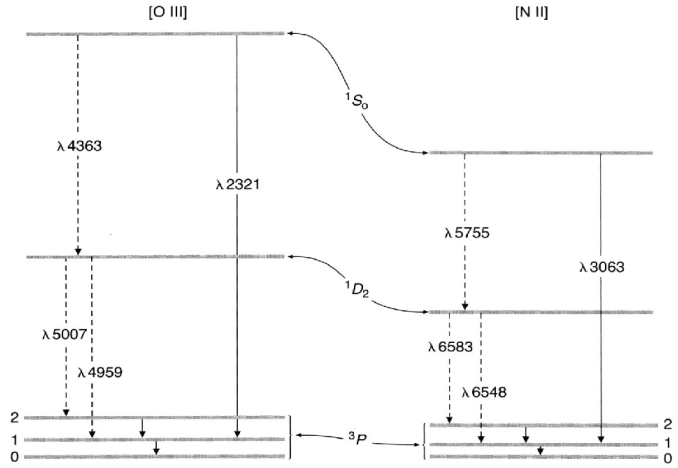

Figure 3.1
Energy-level diagram for lowest terms of [O III], all from ground $2p^3$ configuration, and for [N III] of the same isoelectronic sequence. Splitting of the ground ^3P term has been exaggerated for clarity. Emission lines in the optical region are indicated by dashed lines, and by solid lines in the infrared and ultraviolet. Only the strongest transitions are indicated.

Temperature sensitive line ratios arise in ions with a suitable ground electronic configuration (typically np^2 or np^4) such that a metastable excited state with a significant energy above the ground level exists. This energy should be significantly larger than kTe, but not so large that the lines become undetectable because the line cannot be excited. Note that the two lines in the ^3P ground term have a density sensitive ratio. [AGN3: 5.2]

Diagnostic line ratios (4)

Royal Observatory of Belgium

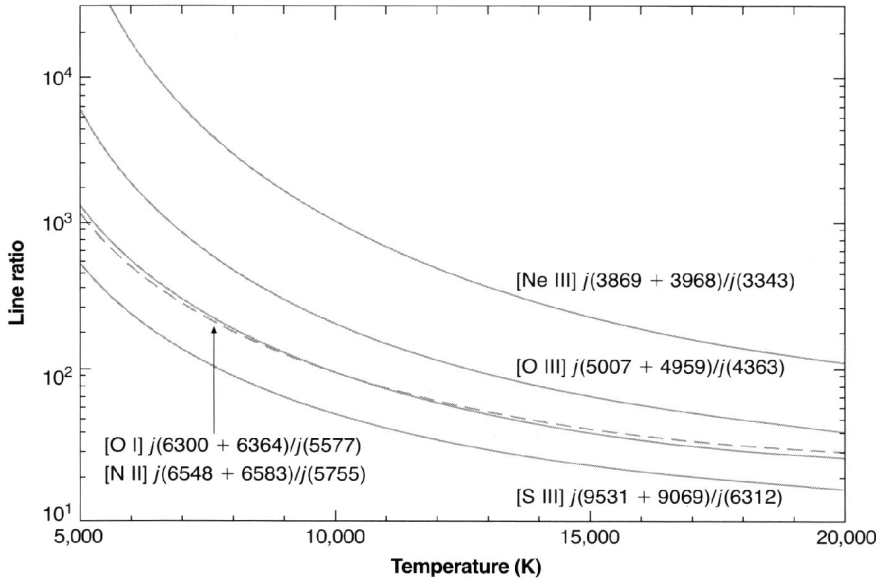

Figure 5.1

Four temperature sensitive forbidden line ratios are shown as a function of the electron temperature. The [O I] (solid line) and [N II] (dashed) ratios are nearly coincident, partially because of their similar excitation potentials. The ratios are shown in the low density limit ($n_e = 1$ cm^{-3}).

$$[\text{O III}]\frac{j_{\lambda4959} + j_{\lambda5007}}{j_{\lambda4363}} = \frac{7.90\exp(3.29 \times 10^4/T)}{1 + 4.5 \times 10^{-4} n_e/T^{1/2}}$$

$$[\text{N II}]\frac{j_{\lambda6548} + j_{\lambda6583}}{j_{\lambda5755}} = \frac{8.23\exp(2.50 \times 10^4/T)}{1 + 4.4 \times 10^{-3} n_e/T^{1/2}}$$

$$[\text{Ne III}]\frac{j_{\lambda3869} + j_{\lambda3968}}{j_{\lambda3343}} = \frac{13.7\exp(4.30 \times 10^4/T)}{1 + 3.8 \times 10^{-5} n_e/T^{1/2}}$$

$$[\text{S III}]\frac{j_{\lambda9532} + j_{\lambda9069}}{j_{\lambda6312}} = \frac{5.44\exp(2.28 \times 10^4/T)}{1 + 3.5 \times 10^{-4} n_e/T^{1/2}}$$

At low densities the line ratio shows a pure exponential dependence on T_e. At high densities, collisional quenching of the ^{1}D and ^{1}S states starts to play a role.

Abundance determination (1)

Royal Observatory of Belgium

Using temperature and density sensitive line ratios, it is possible to derive the electron temperature and density in the ionized gas.

Once these are known, you can calculate ionic abundances by comparing the strength of a collisionally excited forbidden line or a recombination line with Hβ:

$$I_{\mathrm{H}\beta} = \frac{1}{4\pi}\int n_p n_e h\nu_{\mathrm{H}\beta}\alpha^{eff}_{\mathrm{H}\beta}(\mathrm{H}^0, T)ds$$

$$I_{\lambda 5876} = \frac{1}{4\pi}\int n(\mathrm{He}^+) n_e h\nu_{\lambda 5876}\alpha^{eff}_{\lambda 5876}(\mathrm{He}^0, T)ds$$

$$I_{\lambda 4686} = \frac{1}{4\pi}\int n(\mathrm{He}^{++}) n_e h\nu_{\lambda 4686}\alpha^{eff}_{\lambda 4686}(\mathrm{He}^+, T)ds$$

$$I_\nu = \frac{1}{4\pi}\int n_i n_e h\nu q_{1,2}(T) b\, ds$$

$$= \frac{1}{4\pi}\int n_i n_e h\nu \frac{8.63\times 10^{-6}}{T^{1/2}}\frac{\Upsilon(1,2)}{\omega_1}\exp(-\chi/kT) b\, ds$$

If you have observed an [O II] line in your spectrum, you can derive the abundance ratio $n(O^+)/n(H^+)$ using this method. If on the other hand you have observed an O II recombination line, you can derive the abundance ratio $n(O^{++})/n(H^+)$. It is commonly assumed that $n(H^+) = n(H)$, giving you the ionic abundance. [AGN3: 5.11]

Abundance determination (2)

Unfortunately the methods using collisionally excited forbidden lines and recombination lines give different answers! The origin of this discrepancy is still unknown. Various explanations have been offered, but none has been convincingly proved.

The first explanation put forward by Peimbert is that there are temperature fluctuations in the line forming region. To explain the observed discrepancies in some sources, very large fluctuations need to be invoked, which is very hard to explain given the thermostat effect.

The second explanation put forward by Liu is that there are very dense and cold knots embedded in the ionized gas. The knots are too cold to collisionally excite forbidden lines, but can still produce recombination lines. His proposal was that the recombination lines are predominantly produced in these knots, while the forbidden lines come from the surrounding hot gas. Such knots are seen in some PNe, but it is not all clear that they could explain the problem in all sources.

Abundance determination (3)

Given this problem, it is generally not recommended to mix collisionally excited and recombination lines in your analysis (though in the case of H and He you have no other choice!).

Collisionally excited lines are much more easily observed than recombination lines. This is because the ionization energy of an ion is spread over many different lines in the radiative cascade, so each line only gets a small fraction. The number of lines that can be excited collisionally is much smaller, so all the energy goes into a small number of lines.

Because of this published abundance analyses tend to be based on collisionally excited forbidden lines.

However, before you can publish an elemental abundance, you are faced with one more problem: usually you miss some ionization stages, either because the ion has no forbidden lines, or because they are in an unobservable wavelength range. This is often dealt with using ionization correction factors (ICF). These are often rather heuristic rules trying to exploit similarities in ionization potential between different ions.

Abundance determination (4)

Royal Observatory of Belgium

Alternatively you could use a photoionization code to determine the ICF. After all the code will predict the full ionization structure, allowing you to derive the ICF.

This however creates a new problem: in order to know the ionization structure, you need to know the spectral energy distribution emitted by the ionizing source. One way out of this could be to match the Q(H) you derived from a Lyα observation to a grid of SED models and determine a suitable SED that way. But that may not always be possible.

A more general solution is to take all the observations you have and make the parameters that you wish to derive free parameters that are varied until the best possible match to the observations is found. This assures that as much information is taken out of your observations as possible.

This method is very computationally demanding and requires a lot of observables to be available in order to be reliable. The photoionization code Cloudy has a built-in parallelized algorithm that can perform this task.

Autoionization / DR (1)

Royal Observatory of Belgium

If the ionizing source emits sufficiently hard photons, it can happen that an electron from an inner (closed) shell gets excited to a higher shell, or is completely removed. Doing this requires a lot of energy since these electrons are very tightly bound. So typically you need an X-ray source to enable this process, but high excitation PNe can also do it.

As an example, we will look at some transitions:

Fe XV: $1s^2 2s^2 2p^6 3s^2\ {}^1S_0 \rightarrow 1s 2s^2 2p^6 3s^2 3p\ {}^1P^o_1$ (1.7304 Å)

Fe XV: $1s^2 2s^2 2p^6 3s^2\ {}^1S_0 \rightarrow 1s 2s^2 2p^6 3s^2 3p\ {}^3P^o_1$ (1.7316 Å)

Fe XVI: $1s^2 2s^2 2p^6 3s\ {}^2S_{1/2} \rightarrow 1s 2s^2 2p^6 3s 3p\ {}^2P^o_{1/2}$ (1.7269 Å)

It is obvious that the outer electrons have very little influence on the transition energy (spectator electrons). As a result all these inner-shell excitation lines (even from different ionization stages) blend together and form an Unresolved Transition Array (UTA). The specific example above is called the Fe Kβ line. [AGN3: 11.2]

Autoionization / DR (2)

Royal Observatory of Belgium

After an inner-shell excitation or ionization, the ion is left in a very highly excited state with an energy much higher than the ionization potential of the ion. In the example shown before, the excited state will have an energy of 7.17 keV, while the ionization potential of Fe^{14+} and Fe^{15+} is 457 and 489 eV, resp. Such states are called autoionizing states and are very shortlived.

When an electron from a higher shell fills the hole in the inner shell, two things can happen: either the transition energy is emitted as a photon (radiative decay) or the energy is removed by a second electron that leaves the ion (autoionization). There is a fixed branching ratio for these two processes.

After this has happened, the ion can still be in an autoionizing state and the process can repeat itself several times. This is called an Auger cascade, which can remove up to 10 electrons in the event of a K-shell ionization of neutral iron.

Auger cascades will produce a well-defined spectrum of photons and electrons that are emitted in the process.

Autoionization / DR (3)

Royal Observatory of Belgium

An ion can have two excited outer-shell electrons such that the combined energy of the two electrons is above the ionization potential of the ion. An example would be the 2s2p state of He I.

Such states are also autoionizing states and can also lead to spontaneous ionization of the ion.

The reverse process of autoionization is called dielectronic recombination (DR): an electron recombines with an ion while simultaneously exciting one of the bound electrons, leaving the recombined ion in an autoionizing state.

If the bound electron that is being excited is an inner-shell electron, we speak of high-T DR. The autoionizing state has a very high energy, so the incoming electron must have been very energetic. This process is only important in high-T plasmas.

If the bound electron that is being excited is an outer-shell electron, we speak of low-T DR. The resulting recombined state is a doubly excited state. [AGN3: 12.2]

Autoionization / DR (4)

Royal Observatory of Belgium

We will discuss low-T DR a bit further using an example. Let us consider DR of C^{++} to C^{+}. If we look at the level list of C II, we can find the following levels:

$2s^2 2p$	$^2P^o_{1/2}$	0.0 cm^{-1}	(ground level)
$2s^2$	$^1S_0$	196664.7 cm^{-1}	(ionization limit)
$2s2p(^3P^o)3d$	$^2D^o_{3/2}$	198425.43 cm^{-1}	(autoionizing state)
$2s2p(^3P^o)3d$	$^2D^o_{5/2}$	198436.31 cm^{-1}	(autoionizing state)

So C II has autoionizing levels just above the ionization limit (only 0.22 eV). These can readily be excited by electrons in a 10 kK plasma. Hence the name low-T DR.

It is now recognized that low-T DR is an important process, but rate coefficients are often missing or are highly uncertain because frequently the doubly excited states have not been observed and their energies are very uncertain.

Charge transfer

Another process determining the ionization structure of the gas is charge transfer, e.g. the following reaction: [AGN3: 2.7]

$O^+ + H \rightarrow O + H^+$

In this example the ionization potentials of H and O are nearly equal, so the reaction shown is slightly exothermic. But the reverse reaction only has an activation barrier of 0.02 eV, so can also easily take place in low-T plasmas. If the charge transfer dominates, it will force the following ionization balance:

$$\frac{n(O^0)}{n(O^+)} = \frac{9}{8}\frac{n(H^0)}{n_p}$$

Another type of charge transfer reaction is:

$O^{++}(3P) + H \rightarrow O^+(4P) + H^+$

This reaction is strongly exothermic, and also leaves O^+ in an excited state. As a result, the inverse reaction will essentially not proceed at nebular temperatures. Charge transfer reactions can have an important effect, but rate coefficients are often unknown.

Other ionization processes

Royal Observatory of Belgium

There are several other processes that can influence the ionization structure of the gas. They will be briefly mentioned here:

- Collisional ionization and its inverse process 3-body recombination. Collisional ionization can be important in very hot plasmas, while 3-body recombination is only important in very dense plasmas ($> 10^{15}$ cm^{-3}). [AGN: 12.4]
- Compton recoil. Collisions with high-energy photons can ionize particles. This requires a very hard spectrum. [AGN3: 11.3]
- Cosmic ray ionization. Collisions with very energetic cosmic ray particles can ionize particles. This is only important in deeply shielded molecular regions. [AGN3: 11.3]
- Charge exchange with grains. This can profoundly influence the degree of ionization in deeply shielded molecular regions.

Radiative pumping (1)

Royal Observatory of Belgium

Radiative pumping can enhance specific lines in the spectrum emitted by the gas. This can be done by either photons from an emission line (line pumping) or by continuum photons (continuum pumping). The continuum photons can come either from the central source or can be diffuse radiation produced in the nebula itself (e.g. grain emission).

We will look at one example of each:

- Bowen fluorescence: this is a line pumping mechanism that pumps permitted O III lines in high excitation PNe. The mechanism also pumps N III lines, but we will not discuss that.
- [N I] pumping: this is a continuum pumping process that enhances forbidden [N I] lines outside the ionized region.

Radiative pumping (2)

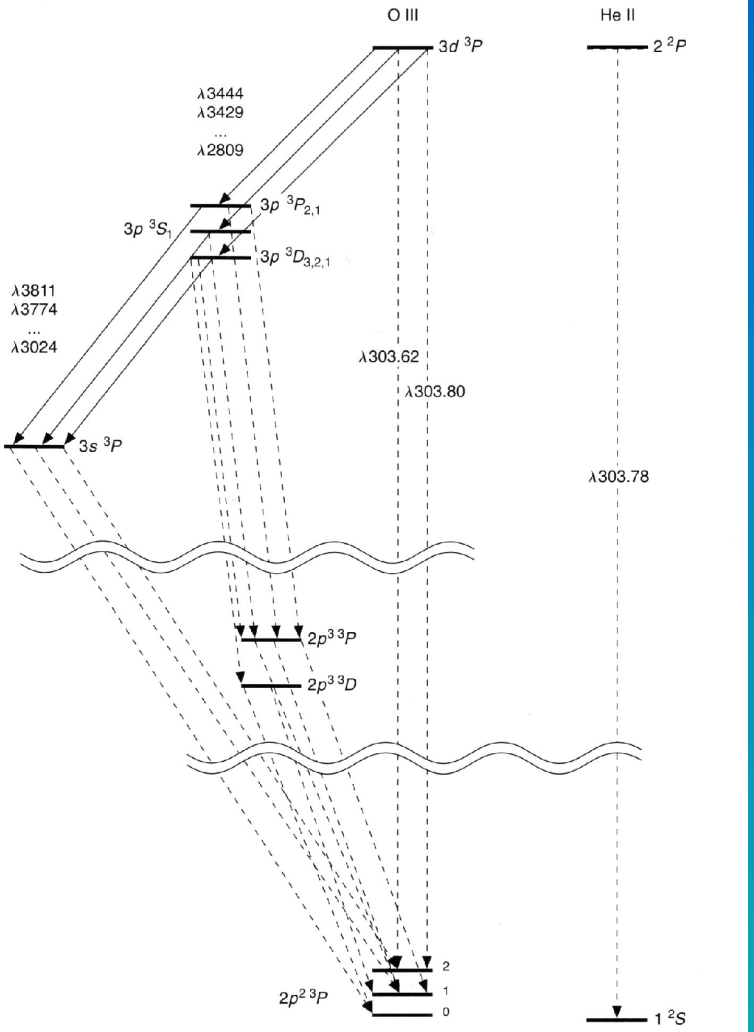

Figure 4.6

Schematized partial energy-level diagrams of [O III] and He II showing coincidence of He II Lα and [O III] $2p^2\ ^3P_2$–$3d\ ^3P\lambda303.80$. The Bowen resonance fluorescence lines in the optical and near-ultraviolet are indicated by solid lines, and the far-ultraviolet lines that lead to excitation or decay are indicated by dashed lines. There are six observable lines in all leading down from $3d\ ^3P^o_2$, and 14 from $3p\ ^3P_{2,1}$, $3p\ ^3S_1$, and $3p\ ^3D_{3,2,1}$, and with relative strengths that can be calculated just from the ratios of transition probabilities.

Probably the best known example of fluoresence is the Bowen mechanism. The He II Lyα line at 303.78 Å nearly coincides with the O III $2p^2\ ^3P_2 \rightarrow 2p3d\ ^3P^o_2$ 303.80 Å line. Each excitation of oxygen is followed by a cascade of allowed O III lines which can often be seen in high excitation PNe.

Note that a small Doppler shift is needed which can have an influence on the yield of this mechanism.

The O III $2p3d\ ^3P^o_2 \rightarrow 2p^2\ ^1D_2$ 323.42 Å downward transition in turn nearly coincides with the N III $2s^22p\ ^2P^o_{1/2} \rightarrow 2s2p(^3P^o)3p\ ^2P_{1/2}$ 323.43 Å line which can subsequently pump N III (not shown).

Radiative pumping (3)

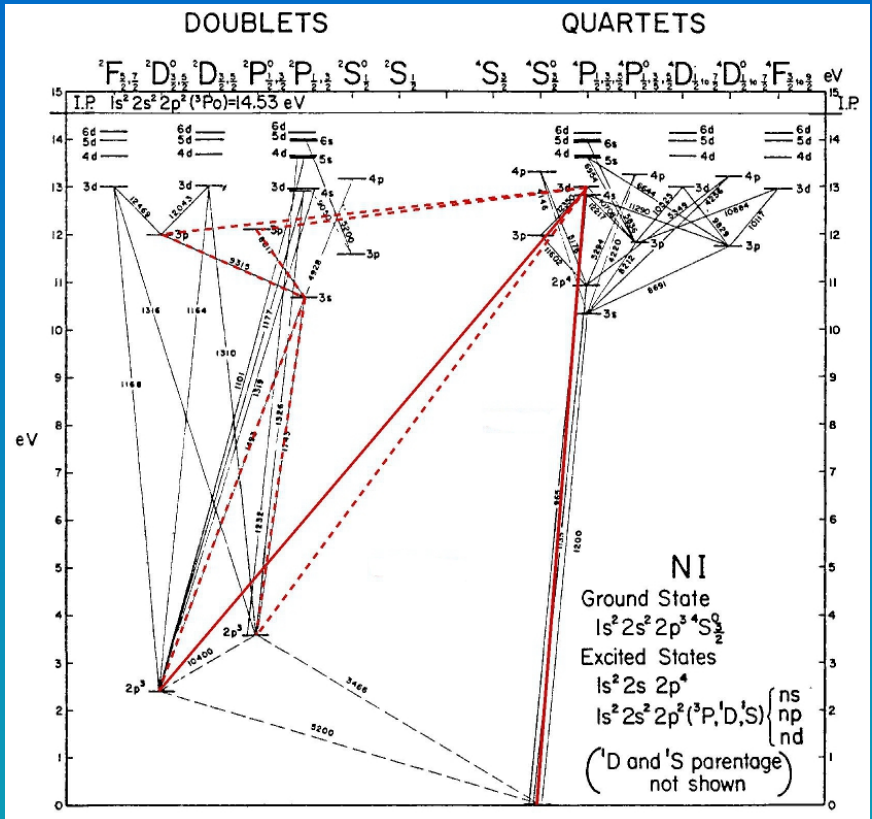

Fig. 72. Partial energy level diagram for atomic nitrogen. Adapted from Tinsley (1972).

Image credit: P. van Hoof, unpublished work

It is often believed that pumping of optical forbidden lines is ineffective because it involves spin-changing (intercombination) transitions. These are forbidden in perfect LS-coupling.

However, in real nature they can be strong, e.g. due to interaction of neighboring terms.

One such system is [N I]. One of several pumping lines is shown here. Continuum pumping is effective here because the driving transition is longward of the Lyman limit. So the pumping can act outside the ionized region where T_e is too low to collisionally excite the [N I] lines. This makes the line emitting region much larger.

Grains (1)

Royal Observatory of Belgium

Grains play an important role in the physics of ionized gas, as well as in the PDR. The main micro-physical processes involving grains are the following:

- Extinction: grains will absorb radiation. Especially in high metallicity environments this can have a substantial influence on the radiative transfer.
- Photoelectric heating: when energetic photons are absorbed, the grain may be ionized (photoelectric effect) and part of the photon energy is carried away by the electron, heating the gas.
- Collisional heating / cooling: when gas particles collide with the grains, they can loose or gain energy, depending on whether the grains are cooler or hotter than the gas.
- Charge exchange: when an ion and a grain collide, the ion may be neutralized by the grain. In rare cases the electron may also move in the opposite direction. This process is very important in fully molecular regions where ions and electrons are rare.

Grains (2)

Royal Observatory of Belgium

- Grain surface reactions: grains may act as catalysts for molecular reactions. The most well known example is the formation of H_2. When a hydrogen atom collides with a grain, it can bond with the grain (physisorption, chemisorption). It can also hop around on the grain from one bonding site to another. That way two H atoms can come together and form an H_2 molecule. This is the dominant formation mechanism as gas phase reactions are very slow. Other reactions can also be sped up considerably by this mechanism.
- Molecule freeze-out: grains can act as seeds for molecular freeze-out, thus removing the molecules from the gas phase and impeding reactions with them. The ice mantles can also change the optical properties of the grains, thus altering the radiative transfer in these regions. This only happens in very cold, fully molecular gas ($T_g < 20$ K).

Stochastic grain heating (1)

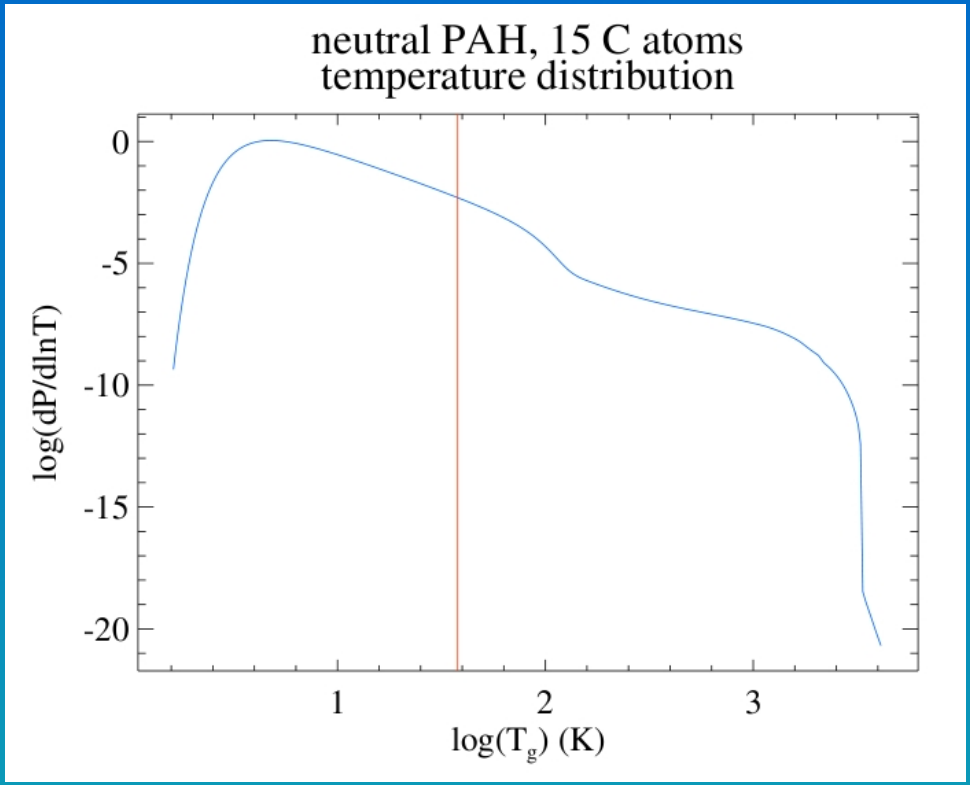

Image credit: P. van Hoof, unpublished work

When a very small grain (VSG, radius less than 100 Å) absorbs a single energetic photon, this will raise the temperature of the grain substantially (by up to several thousand kelvin) since the enthalpy of the grain is very small. The grain will then start to radiatively cool until the next photon is absorbed. If that takes a long time, the grain may cool to very low temperatures. Given the grain enthalpy, the grain optical properties, and the incident spectrum, you can calculate what the probability distribution over temperature of the grain will be. The red vertical line indicates the equilibrium temperature.

Stochastic grain heating (2)

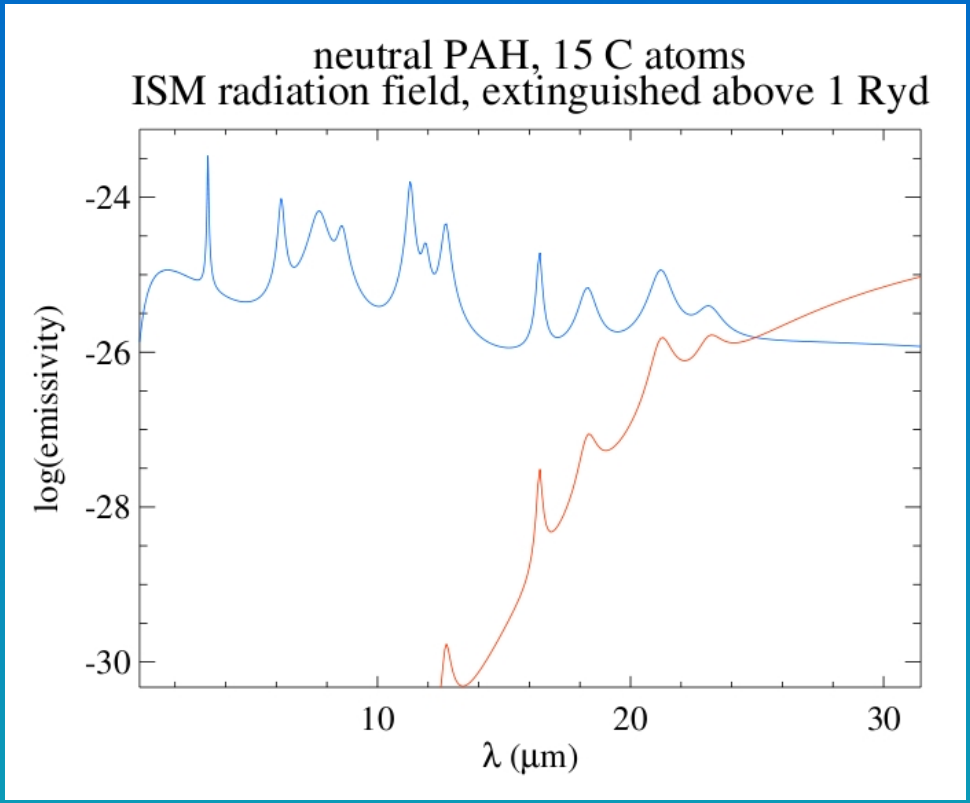

Image credit: P. van Hoof, unpublished work

Since thermal emission is a very non-linear function of temperature (exponential in the Wien tail) having these brief excursions to high temperatures significantly alters the emitted spectrum, even after averaging over time. The short wavelength end of the spectrum (blue curve) will be much stronger compared to the assumption that the grains are constantly at the equilibrium temperature (red curve). This is an important effect in the ISM.

Royal Observatory of Belgium

Determining the physical conditions (1)

Royal Observatory of Belgium

In a photoionization code like Cloudy, all the processes discussed so far need to be balanced to obtain a steady-state solution in thermal equilibrium. This is done in a nested set of solvers:

Assume gas density

- Assume electron temperature
  - Assume electron density
    - Solve the ionization structure
    - Determine the electron density from ionic abundances
  - Iterate until assumed and determined electron density match
  - Calculate the heating and the cooling
- Iterate until the heating and cooling match
- Calculate the pressure

Iterate until constant pressure is achieved

Determining the physical conditions (2)

Royal Observatory of Belgium

The outermost solver is only exercised in a constant pressure model. In a model with a prescribed density law, such as a constant density model, only the inner three solvers are used.

This nested iteration needs to be done for each zone. Once it has converged, it is possible the determine the opacity in that zone, e.g. photoionization cross sections of various ions and from grains.

When the opacities are known, radiative transfer can be done and the radiation field for the next zone can be determined. This will also include spherical dilution effects.

Now the solvers can be exercised again for the next zone, etc. This way the code will gradually work itself outwards until some stopping criterion is fulfilled (e.g. T_e dropping below some preset value, a preset column density being reached, etc.).

Now the total line and continuum opacities are known. These are needed to calculate the escape probabilities. Normally there will be another layer of iteration to converge the line and continuum opacities.

Basic PDR physics (1)

Royal Observatory of Belgium

The physics of PDRs is a very rich subject that could easily warrant a separate presentation. Here I will only briefly touch on three important subjects.

The Solomon process. The H_2 molecule is symmetrical. As a result there are no permitted ro-vibrational transitions in the electronic ground state of H_2. In other words, all ro-vibrational transitions of H_2 are forbidden and very weak. As a result, the main route for destruction of H_2 is not direct photodissociation, but the Solomon process. This is an indirect destruction process. The first step is the absorption of a UV photon exciting H_2 into an electronically excited state. Balmer continuum photons can do that. Subsequently H_2 can decay into the continuum of the ground electronic state, dissociating the molecule.

The photons that are responsible for the Solomon process need to be shielded before significant H_2 formation can start. This is done mainly through carbon photoionization and H_2 self-shielding.

Basic PDR physics (2)

Royal Observatory of Belgium

C-rich vs. O-rich chemistry. After H_2, the first molecule that forms is CO. This is because CO is a very stable molecule that can exist at very high temperatures (it is present in the solar photosphere).

The formation of CO is very efficient and it tends to lock up all the available C or O.

This implies that in O-rich objects, after the CO formation is complete, only O will be available to form other molecules, e.g. OH, H_2O and various other oxydes (e.g. SiO).

In C-rich objects on the other hand, only C will be available to form other molecules, such as C_2, C_3, and various carbides (e.g. SiC).

As a result the chemistry in O-rich and C-rich objects is very different. Such objects will form different molecules and also different types of grains. Note however that especially in high excitation PNe, high energy photons can penetrate into the PDR, which can keep CO partially dissociated (see also next slide). This makes the distinction less clear-cut in such objects.

Basic PDR physics (3)

Royal Observatory of Belgium

X-ray PDRs or XDRs. The ionized region which is in between the PDR and the ionizing source will tend to absorb all the ionizing radiation.

However, the photoionization cross section varies $\sim \nu^{-3}$ which implies that the absorption will be most efficient near the threshold.

If you have a very high excitation source, such as a hot PN central star, or an X-ray source. It can happen that at the “ionization boundary” not all the X-ray photons have been absorbed away simply because the cross section is too low at those energies.

The X-ray photons penetrate deeper and keep the gas partially ionized even beyond the “ionization boundary”. The concept of such a boundary starts to break down: there is a gradual change instead.

The energetic photons that penetrate into the PDR cause significant changes in the chemistry because the gas is partially ionized. Also the PDR gas is hotter because of the energetic electrons resulting from the ionizations.

To indicate these differences, one often speaks of XDRs. Remember however that PDRs and XDRs are not fundamentally different!

Some applications of Cloudy (1)

Royal Observatory of Belgium

Cloudy is very flexible and can read commands from an input script, which makes it easy to configure:

```
title PN model
sphere
cosmic rays background
TABLE STAR RAUCH SOLAR 5.192248 LOG 8.000000
LUMINOSITY 37.326397 LOG range -0.000232 6.866524
RADIUS= 16.035376 LOG
DLAW 4.518836 1.381056
abundances planetary no grains
ELEMENT HELI ABUNDANCE 10.893871 LOG
ELEMENT CARB ABUNDANCE 8.840264 LOG
ELEMENT NITR ABUNDANCE 8.245247 LOG
ELEMENT OXYG ABUNDANCE 8.636869 LOG
ELEMENT NEON ABUNDANCE 7.984562 LOG
ELEMENT MAGN ABUNDANCE 7.214100 LOG
ELEMENT SILI ABUNDANCE 5.911162 LOG
ELEMENT SULP ABUNDANCE 6.929121 LOG
ELEMENT CHLO ABUNDANCE 5.192172 LOG
ELEMENT ARGO ABUNDANCE 6.054798 LOG
ELEMENT CALC ABUNDANCE 4.328190 LOG
ELEMENT IRON ABUNDANCE 5.862868 LOG
GRAIN ABUND=-0.064086 LOG ISM GRAPHITE
GRAIN ABUND=0.098686 LOG PAH
print line flux seen at earth
print line faint -15
distance 790 linear parsec
atom H-like levels 20 element hydrogen
atom H-like levels 15 element helium
stop line "CO  " 216.9m reaches 1.519e-3
stop zone 3000
stop temperature 10 K linear
stop radius 17.3
set drmin 0.000001 linear relative
iterate
save physical cond ".phy"
save leiden ".lei"
save molecules ".mol"
```

Image credit: P. van Hoof.

Some applications of Cloudy (2)

Royal Observatory of Belgium

The output contains lots of information on the model that was produced. Far too much to show here. Below is a brief excerpt of the emission line predictions of the model from the previous slide.

H	1	1216A	-7.960	6.7955	CN	440.7m	-16.725	0.0000	Ne 5	101.1A	-12.213	0.0004	Fe 6	160.8A	-12.138	0.0005
H	1	1026A	-11.057	0.0054	CN	440.6m	-16.652	0.0000	Ne 5	97.08A	-13.013	0.0001	Fe 6	144.2A	-11.932	0.0007
H	1	972.5A	-11.179	0.0041	CN	378.5m	-18.794	0.0000	Ne 5	104.8A	-11.723	0.0012	Fe 6	158.7A	-11.992	0.0006
H	1	949.7A	-11.234	0.0036	CN	377.8m	-16.837	0.0000	Ne 5	94.96A	-13.221	0.0000	Fe 6	176.6A	-12.054	0.0005
H	1	937.8A	-11.272	0.0033	CN	377.7m	-16.775	0.0000	Ne 5	103.1A	-11.852	0.0009	Fe 6	198.0A	-11.924	0.0007
H	1	930.8A	-11.297	0.0031	CN	331.2m	-19.048	0.0000	Ne 5	92.60A	-13.324	0.0000	Fe 6	138.1A	-11.974	0.0007
H	1	926.2A	-11.319	0.0030	CN	330.6m	-16.969	0.0000	Ne 5	102.0A	-12.287	0.0003	Fe 6	185.1A	-11.996	0.0006
H	1	923.2A	-11.341	0.0028	CN	330.5m	-16.915	0.0000	Ne 5	105.2A	-11.936	0.0007	Fe 6	279.2A	-11.479	0.0021
H	1	921.0A	-11.367	0.0027	CN	294.4m	-19.301	0.0000	Ne 5	92.17A	-13.526	0.0000	Fe 6	135.7A	-12.047	0.0006
H	1	919.4A	-11.395	0.0025	CN	293.9m	-17.117	0.0000	Ne 5	101.3A	-12.217	0.0004	Fe 6	135.7A	-12.094	0.0005
H	1	918.1A	-11.423	0.0023	CN	293.8m	-17.069	0.0000	Ne 5	106.3A	-12.029	0.0006	Fe 6	141.9A	-12.117	0.0005
H	1	917.2A	-11.441	0.0022	CN	265.0m	-19.557	0.0000	Ne 5	92.79A	-13.985	0.0000	Fe 6	134.0A	-12.184	0.0004
H	1	916.4A	-11.454	0.0022	CN	264.5m	-17.277	0.0000	Ne 5	93.66A	-14.063	0.0000	Fe 6	296.2A	-11.630	0.0015
H	1	915.8A	-11.461	0.0021	CN	264.5m	-17.234	0.0000	Ne 5	103.2A	-12.641	0.0001	Fe 6	189.1A	-12.243	0.0004
H	1	915.3A	-11.466	0.0021	CN	241.0m	-19.814	0.0000	Ne 6	122.9A	-11.018	0.0059	Fe 6	134.0A	-12.287	0.0003
H	1	914.9A	-11.468	0.0021	CN	240.5m	-17.449	0.0000	Ne 6	400.0A	-10.966	0.0067	Fe 6	178.8A	-12.319	0.0003
H	1	914.6A	-11.468	0.0021	CN	240.5m	-17.410	0.0000	Ne 6	999.2A	-12.383	0.0003	Fe 6	134.6A	-12.264	0.0003
H	1	914.3A	-11.464	0.0021	CN	220.9m	-20.076	0.0000	Ne 6	111.4A	-11.414	0.0024	Fe 6	138.2A	-12.307	0.0003
H	1	914.0A	-11.450	0.0022	CN	220.5m	-17.634	0.0000	Ne 6	98.44A	-11.653	0.0014	Fe 6	155.7A	-12.491	0.0002
H	1	6563A	-8.344	2.8051	CN	220.5m	-17.598	0.0000	Ne 6	114.6A	-11.472	0.0021	Fe 6	220.7A	-12.225	0.0004
H	1	4861A	-8.792	1.0000	CN	204.0m	-20.342	0.0000	Ne 6	561.8A	-11.389	0.0025	Fe 6	158.8A	-12.458	0.0002
H	1	4340A	-9.118	0.4718	CN	203.6m	-17.829	0.0000	Ne 6	90.23A	-13.309	0.0000	Fe 6	155.5A	-12.544	0.0002
H	1	4102A	-9.377	0.2599	CN	203.5m	-17.796	0.0000	Ne 6	432.0A	-11.207	0.0038	Fe 6	135.7A	-12.489	0.0002
H	1	3970A	-9.593	0.1583	CN	189.4m	-20.615	0.0000	Ne 6	89.75A	-13.613	0.0000	Fe 6	187.8A	-12.543	0.0002
H	1	3889A	-9.775	0.1041	CN	189.1m	-18.035	0.0000	Ne 6	109.6A	-11.483	0.0020	Fe 6	144.0A	-12.597	0.0002
H	1	3835A	-9.926	0.0735	CN	189.0m	-18.005	0.0000	Ne 6	138.8A	-11.314	0.0030	Fe 6	186.3A	-12.713	0.0001
H	1	3798A	-10.048	0.0554	CN	176.8m	-20.894	0.0000	Ne 6	101.4A	-11.966	0.0007	Fe 6	215.4A	-12.527	0.0002
H	1	3771A	-10.148	0.0441	CN	176.5m	-18.253	0.0000	Ne 6	86.34A	-13.724	0.0000	Fe 6	134.0A	-12.752	0.0001
H	1	3750A	-10.235	0.0361	CN	176.5m	-18.225	0.0000	Ne 6	82.42A	-13.931	0.0000	Fe 6	144.2A	-12.725	0.0001
H	1	3734A	-10.316	0.0299	CN	165.8m	-21.182	0.0000	Ne 6	89.86A	-13.502	0.0000	Fe 6	201.5A	-12.708	0.0001
H	1	3722A	-10.395	0.0249	CN	165.5m	-18.484	0.0000	Ne 6	101.6A	-12.049	0.0006	Fe 6	155.1A	-12.907	0.0001
H	1	3712A	-10.472	0.0209	CN	165.5m	-18.458	0.0000	Ne 6	84.16A	-14.027	0.0000	Fe 6	217.8A	-12.704	0.0001
H	1	3704A	-10.544	0.0177	CN	156.1m	-21.483	0.0000	Ne 6	102.7A	-12.336	0.0003	Fe 6	158.9A	-12.907	0.0001
H	1	3697A	-10.613	0.0151	CN	155.8m	-18.732	0.0000	Ne 6	82.10A	-14.121	0.0000	Fe 6	138.2A	-12.956	0.0001
H	1	3692A	-10.675	0.0131	CN	155.8m	-18.707	0.0000	Ne 6	90.94A	-13.591	0.0000	Fe 6	138.3A	-12.976	0.0001
H	1	3687A	-10.729	0.0116	CN	147.5m	-21.803	0.0000	Ne 6	82.81A	-14.238	0.0000	Fe 6	185.2A	-13.072	0.0001
H	1	3683A	-10.767	0.0106	CN	147.2m	-19.001	0.0000	Ne 6	82.64A	-14.298	0.0000	Fe 6	134.6A	-13.153	0.0000
H	1	1.875m	-9.318	0.2983	CN	147.2m	-18.978	0.0000	Ne 6	79.16A	-14.514	0.0000	Fe 6	192.0A	-13.137	0.0000

Image credit: P. van Hoof.

Some applications of Cloudy (3)

Royal Observatory of Belgium

This plot shows the electron temperature and density as a function of depth predicted by Cloudy

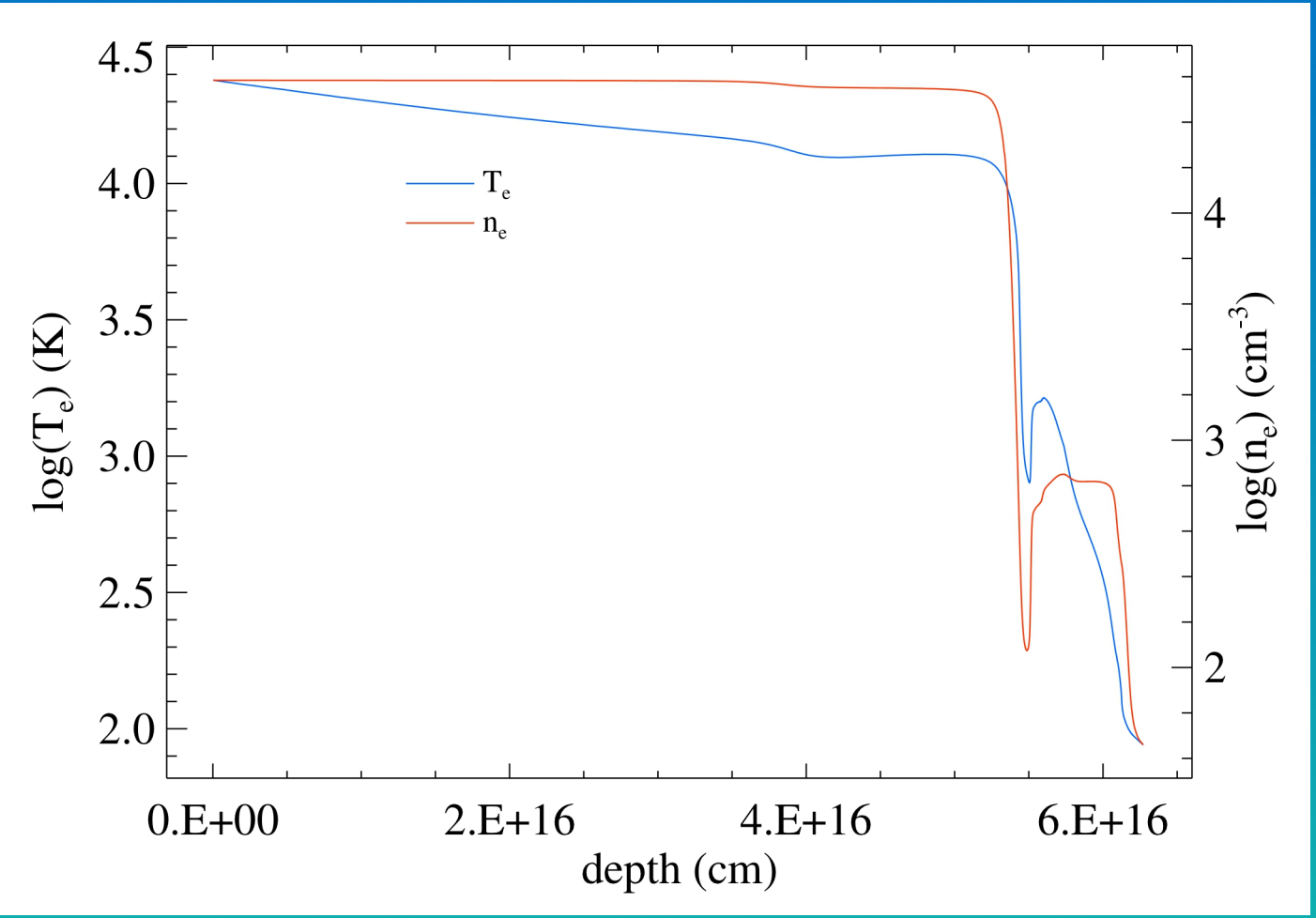

Image credit: P. van Hoof.

Some applications of Cloudy (4)

Royal Observatory of Belgium

This plot carbon structure in a model of the Orion blister. This is one of the first unified models of an ionized region and a PDR that we produced.

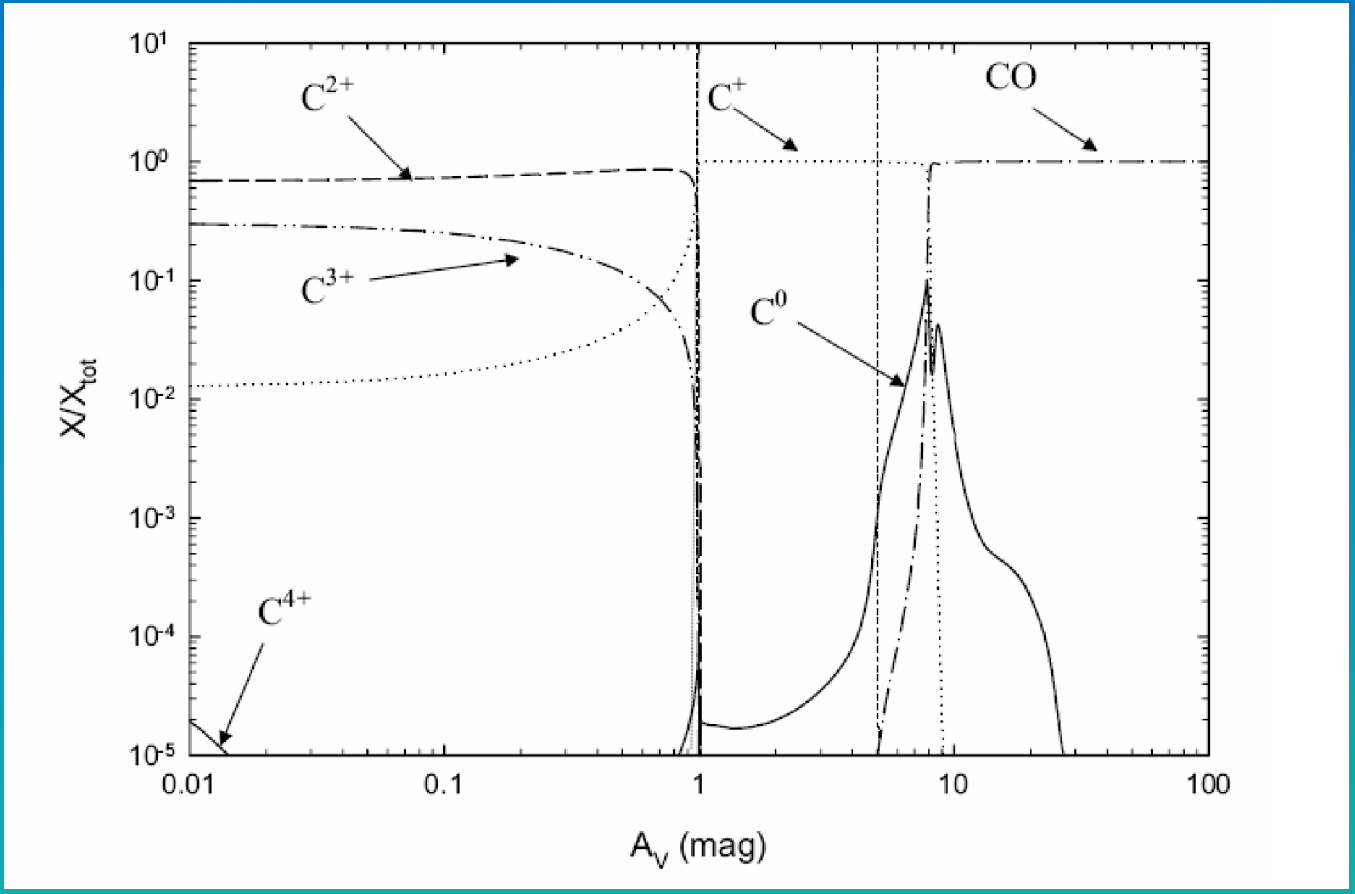

Image credit: Abel et al., 2005, ApJS 161, 65

Some applications of Cloudy (5)

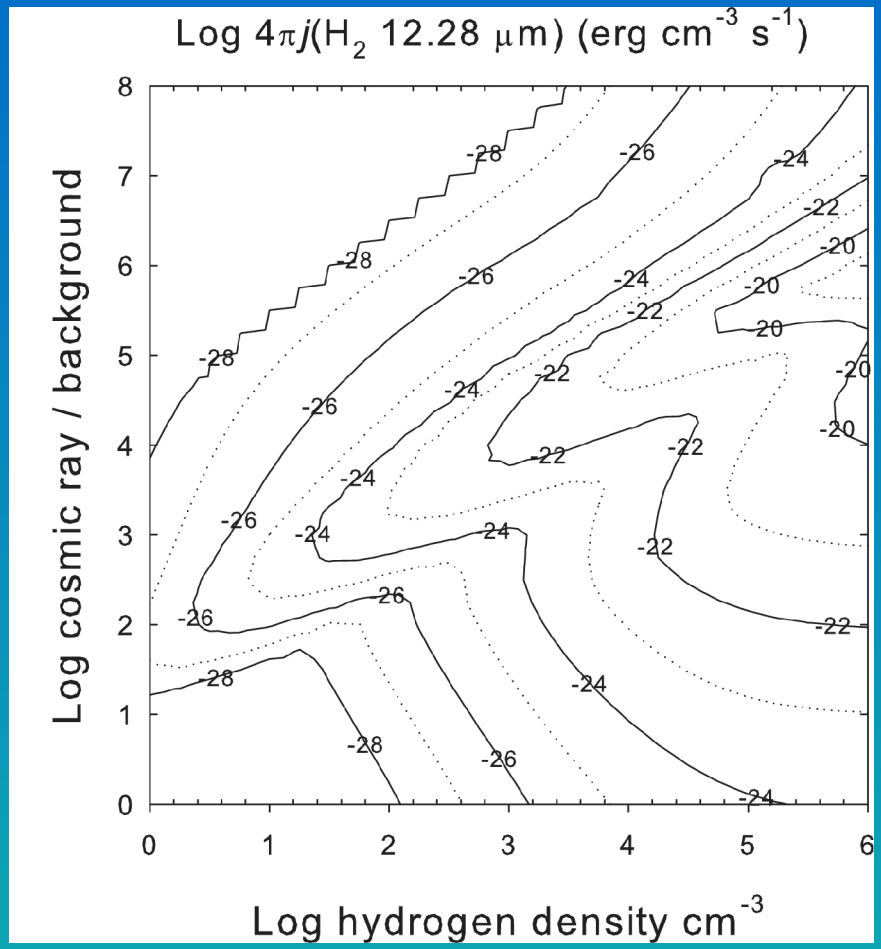

Image credit: Ferland et al., 2009, MNRAS 392, 1475.

This image highlights the capability of Cloudy to generate grids of models. These grids can be used to generate plots of one of the model quantities (in this case the H_2 12.28 μm flux) as a function of the parameters that were varied (in this case the gas density and the cosmic ray density).

In this case the plot was used to investigate the mechanism that heats the optical filaments seen in galaxy clusters.

Cloudy_3D

Royal Observatory of Belgium

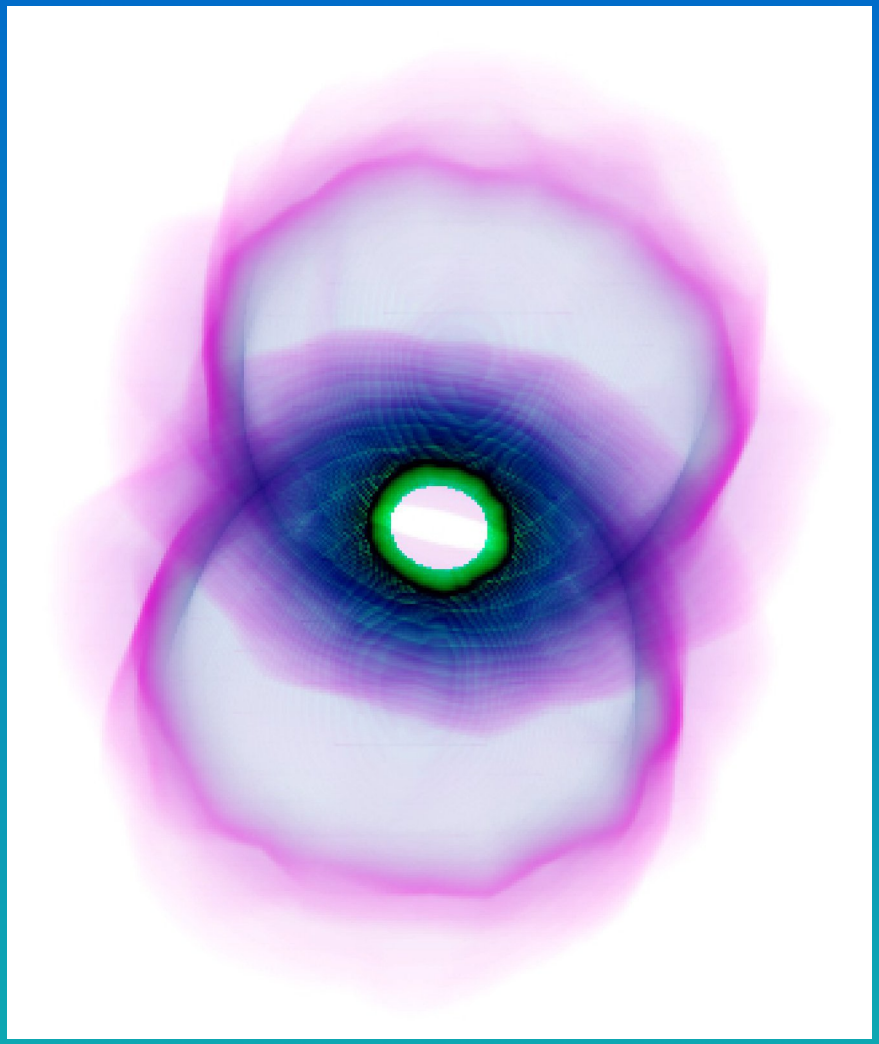

Image credit: Christophe Morisset.

It is possible to generate 3D models of nebulae using the code Cloudy_3D written by Christophe Morisset. This is done by calculating many 1D rays with Cloudy and then combining these with Cloudy_3D to generate a 3D image. On the left is an image of a bipolar PN produced with Cloudy_3D. This is a 450^3 cube image obtained from 600 Cloudy runs. Red is [O II], green is [O III], and blue is Hα.

http://sites.google.com/site/cloudy3d/

The future (1)

Royal Observatory of Belgium

A complex code like Cloudy is never finished. It is continually being updated. Being an open source code, we always welcome 3rd party contributions to the code! Many people have contributed in the past. At this moment the main developers of the code are Gary J. Ferland, Ryan L. Porter, Robin J.R.W. Williams, and Peter A.M. van Hoof.

Development in the near future will be aimed at:

- Updating and extending the atomic and molecular data. The upcoming release will have the LAMDA database and we are also working on including molecular data from the CDMS and JPL databases. We are also working on including the Chianti database.
- Parallellizing the code. This will be done in MPI. The upcoming release will have the capability to run grids and optimizations on distributed MPI clusters.
- Running the code on GPUs. This is still in its infancy.
- Updating the molecular solver. This project is nearing completion and should be included in the C12 release. This version will be much more stable.

The future (2)

Royal Observatory of Belgium

In the longer run we will be working on these goals:

- Moving the code to exact and full 3D radiative transfer. This is a challenging task as it requires a fundamental redesign of the code. It is also computationally very demanding.
- Merging photoionization and hydrodynamics codes. It is very clear that in the future we will need a code that can do both photoionization and hydrodynamics as the two are intimately linked. However, doing full photoionization and hydrodynamics simultaneously is computationally too demanding. So current codes either do full hydro with very simple photoionization, or full photoionization with simplified hydro. Cloudy currently has an experimental feature where it can model advection flows, like the one that exists in the Orion blister.
- Move towards time dependence. In photoionized regions assuming a time-steady situation is usually OK (though exceptions exist), but in PDRs the validity of this assumption is far more questionable. Chemical reactions can be very slow at ISM densities, so including time dependence here would be warranted.

Royal Observatory of Belgium

Thanks!

Thank you very much for your attention and have a safe journey home!

This presentation is available for download at:

http://homepage.oma.be/pvh/winterschool/

Fur further reading:

http://www.agn3.org/

To download the Cloudy code:

http://www.nublado.org/

To download the Cloudy_3D code:

http://sites.google.com/site/cloudy3d/